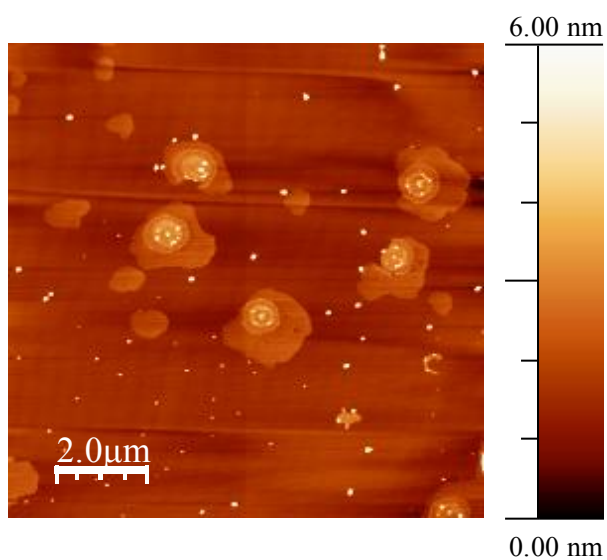***Graphical Abstract**

Unusual flexibility of mesophase pitch-derived carbon materials: An approach to the synthesis of graphene

D. Barreda, A.M. Pérez-Mas, A. Silvestre-Albero, M.E. Casco, C. Herdes, S. Rudić, E.A. Müller, C. Blanco, R. Santamaria, J. Silvestre-Albero, F. Rodríguez-Reinoso

GRAPHICAL ABSTRACT

A simple route for the synthesis of graphene-flakes has been described based on the unusual flexibility of petroleum pitch-derived carbons

Unusual flexibility of mesophase pitch-derived carbon materials: An approach to the synthesis of graphene

D. Barreda,[a] A.M. Pérez-Mas,[a] A. Silvestre-Albero,[b] M.E. Casco,[b] S. Rudić,[c] C. Herdes,[d,e] E.A. Müller,[d] C. Blanco,[a] R. Santamaria,[a,*] J. Silvestre-Albero,[b,*] and F. Rodríguez-Reinoso[b]

[a]Instituto Nacional del Carbón (INCAR-CSIC), Apdo. 73, 33080 Oviedo, Spain
[b]Laboratorio de Materiales Avanzados, Departamento de Química Inorgánica, Universidad de Alicante, E-03690 San Vicente del Raspeig, Spain
[c]ISIS Facility, Rutherford Appleton Laboratory, Chilton, Didcot, OX11 0QX, UL.
[d]Department of Chemical Engineering, Imperial College London, South Kensington Campus, London SW7 2AZ, UK
[e]Department of Chemical Engineering, University of Bath, Claverton Down, Bath, Somerset BA2 7AY, UK.

Abstract

Structural flexibility in a petroleum pitch-derived carbon material has been indirectly evaluated using X-ray diffraction (XRD), immersion calorimetry and inelastic neutron scattering (INS) measurements. Exposure of the carbon material to an organic solvent (e.g., n-nonane) gives rise to a large internal rearrangement, associated with a drastic re-ordering of the graphitic microdomains. These structural changes are also associated with a high flexibility of the internal porous network, as observed by inelastic neutron scattering measurements. The internal rearrangement and the structural flexibility could be responsible for the excellent performance of this kind of activated carbons in a wide variety of adsorption processes. Last but not least, the structural characteristics of these carbon materials composed of graphitic microdomains has been used to synthesize graphene "egg-like" flakes following a simple procedure based on exfoliation with organic solvents.

*Corresponding author:

Dr. Joaquín Silvestre-Albero, Email: joaquin.silvestre@ua.es

Dr. Ricardo Santamaria, Email: riqui@incar.csic.es

1. Introduction

Nanoporous materials with a well-developed porous structure and surface chemistry constitute one of the main pillars in nanotechnology. These solids include zeolites, activated carbons, ordered-mesoporous silicas (OMS), metal-organic frameworks (MOF), among others. One of the main concerns in the design and synthesis of these nanoporous materials is the knowledge of their porous structure, since the size and the shape of the pore cavities will define their performance in a given application (for instance in gas adsorption/separation processes, as a sensor, in drug delivery processes, as a catalyst, etc.). Traditionally, the porous structure of nanoporous solids has been evaluated by gas adsorption at cryogenic temperatures (e.g., N_2 at 77 K and Ar at 87 K) [1,2]. Assuming a rigid structure for the porous solid, the monolayer formation in the surface can be used to estimate the "apparent" surface of the material after application of the corresponding mathematical equations (e.g., BET equation). However, it is well known that this assumption is not always accurate for certain nanoporous solids due to the presence of adsorption-induced deformation phenomena upon an external stimuli (e.g., pressure and/or temperature changes, exposure to a certain probe molecule, etc.). Whereas this phenomenon has been widely established for MOFs (for instance the gate-opening effect in ZIF-8 or MIL-53) [3,4], it is sometimes neglected in the evaluation and understanding of other porous solids. These structural changes are due to the substantial stress that takes place in the inner cavities of the solid upon adsorption (in the order of GPa), thus giving rise to contractions, swelling and morphological transitions. For instance, Monte Carlo simulations for methane adsorption in slit-shaped carbon narrow micropores (0.315 nm in size) provided an *adsorption stress* or *solvation pressure ca*. 1.8 GPa at 19 MPa [5]. Similar studies of argon in carbon-slit nanopores suggest an enhancement of the tangential pressure of ~ 20 000 times the normal bulk

pressure [6]. Interestingly, these phenomena are not exceptional and have been identified for a wide range of materials including activated carbons [5-10], mesoporous silicas [11], zeolites [12], etc. Despite the relevance of these adsorption-induced phenomena defining the final porous structure under *operando* conditions and consequently, the final performance of the nanoporous system, their presence has been traditionally neglected due to the difficulty in assessing these structural changes, particularly in amorphous systems such as carbon materials. For instance, *in-situ* dilatometry measurements performed in mesoporous silicas and carbon materials upon adsorption suggest that these structural characteristics depends on the adsorbate used, the adsorption temperature and the pore size, these changes being rather small (swelling not exceeding 1%) [9,13]. These findings have been corroborated by mathematical calculations using density functional theory (DFT) and Monte Carlo simulations.

Recent reports described in the literature point to activated carbons derived from petroleum residues as being among the highest performing materials to date for a wide range of applications ranging from high-pressure methane storage, CO_2 capture, benzene and toluene adsorption, energy storage in electric double layer capacitors, etc., surpassing conventional activated carbon materials [14-16]. This outstanding performance has been rationalized by the presence of a highly developed porous structure (narrow micropore volume above 1 cm^3/g) and a BET surface exceeding 3200 m^2/g. The crux of the matter is that these metrics obtained for a carbon derived from a graphitizable residue cannot be exclusively justified considering a perfectly rigid arrangement of graphitic crystallites. Furthermore, the large BET surface area achieved exceeds the theoretical value for a single graphene layer (2630 m^2/g), shedding a shadow on the above-mentioned results.

The main goal of the present work is to evaluate the presence of structural changes in petroleum-pitch derived activated carbons upon adsorption of different organic molecules (including crystallite reorientation and swelling/contraction phenomena) and to determine if it is this aspect of the material that accounts for the exceptionally high adsorption performance. As an ancillary result, the unexpectedly high flexibility in these materials will be exploited to synthesize graphene. Compared to conventional processes for graphene production, e.g., via oxidation followed by exfoliation/thermal reduction of graphite, the present proposed method, based on an exfoliation treatment with N-methyl-2-pyrrolidone (NMP), constitutes a simple and expedite approach.

2. Experimental Section

2.1. Preparation of the carbon sample

The activated carbon evaluated in this study was prepared from a petroleum mesophase pitch (PP) obtained from a vacuum residue (VR). The mesophase pitch and the KOH (KOH:precursor ratio of 6:1 (w/w)) were initially mixed in a ball mill for 30 min, and subsequently submitted to an activation treatment in a horizontal furnace at 1073 K for 2h, under a nitrogen flow (100 mL/min). The as-synthesized material was washed with 10% HCl solution and distilled water until complete removal of the chloride ions.

2.2. X-ray diffraction measurements

X-ray diffraction measurements of the activated carbon before and after chemical treatment with n-nonane and methylene blue were performed using a Bruker D8-Advanced equipment with a KRISTALLOFLEX K 760-80F X-ray generator and a

copper anode (λ= 1.54056 Å). Pre-impregnation with n-nonane was performed using an excess of the liquid to saturate the sample, followed by an overnight outgassing treatment at 298 K to selectively remove the excess of n-nonane from large pores, as described elsewhere [17]. Under these conditions only narrow micropores (those below 1 nm) remain filled with n-nonane. Methylene blue (MB) pre-impregnation was performed in aqueous phase using the standard ASTM method.

2.3. Immersion calorimetry measurements

Immersion calorimetry measurements were performed in a Tian-Calved C-80D calorimeter at 303 K. A full description of the experimental set-up can be found elsewhere [18]. Before the immersion calorimetry measurements with benzene and alpha-pinene, activated carbons were outgassed at 523 K for 4h.

2.4. INS measurements

Inelastic neutron scattering (INS) experiments were performed using the TOSCA spectrometer at the ISIS Neutron and Muon Pulsed Source, Rutherford Appleton Laboratory in the UK [19]. Before the experiment, 1.0 g of activated carbon was pre-adsorbed with the appropriate amount of liquid n-nonane to completely fill the pore cavities (total pore volume was obtained from the N_2 adsorption isotherms at 77 K). The pre-impregnated sample was wrapped in Al-foil and loaded into the high-pressure stainless steel cell supplied by ISIS. INS measurements were done at 4 K. After the first experiment with the saturated sample, the system was pumped under vacuum at 298 K for 4h to remove n-nonane from large cavities [17]. To end up, the sample was pressurized with methane gas (6 MPa) at 275 K for 3h before cooling down to 4 K using a closed cycle refrigerator (CCR).

Computational analysis of INS data was done using the mixed Monte Carlo multiple minimization and Large Scale low mode method, as implemented in the MacroModel software (Schrödinger), until no additional new structures were obtained. All conformations of n-nonane with relative energies $\leq$ 7.8 kJ/mol were subsequently submitted for geometry optimization using the Gaussian 09 suite of programs [20] and density functional theory (DFT) at the B3LYP/6-311++G(d,p) level. This led to a new set of relative energies (corrected to zero point energies), molecular structures and (harmonic) vibrational spectra, which could then be compared with experiment. More accurate energies were calculated for the optimized DFT structures, at the MP2/6-311++G(d,p) level of theory. All energies were corrected for zero point energy using the un-scaled DFT harmonic frequencies. The theoretical inelastic neutron scattering (INS) transition intensities were derived from the calculated normal mode eigenvectors, and the corresponding spectra were simulated using the aCLIMAX program [21].

2.5. Molecular simulations

Classical Molecular Dynamics simulations were performed using the coarse-grained SAFT forcefield [22,23]. An empty rigid graphitic pore of 1 nm was exposed to an excess of nonane molecules at 275 K until pore filling was achieved. The resulting system was then exposed to a reservoir of methane molecules and the pressure increased by compressing the bulk volume until a pressure of 6 MPa was achieved. More information can be found in the Supporting Information.

2.6. Preparation of graphene from PP-AC

PP-AC carbon was dispersed using two different organic solvents, N-methyl-2-pyrrolidinone (NMP, spectroscopic grade, Aldrich) and N,N-dimethylformamide

(DMF), at a concentration of 5 mg/ml (200 mL, round-bottomed flask). The dispersion was then sonicated (Bransonic Ultrasonic 5510-MTH, 135 W-42 kHz) for 15 min.

2.6. Atomic force microscopy

The lateral size and the height of the synthesized graphene was measured using AFM imaging and profiling by depositing a drop of a water suspension of each sample onto a surface of mica. The graphene sheets were imaged using a Dulcinea atomic force microscope from Nanotec ElectronicaTM operating under ambient conditions.

3. Results and discussion

Complete characterization of the PP-AC sample has been described elsewhere [14,15]. Briefly, the petroleum-pitch derived activated carbon (PP-AC) selected for this study exhibits a BET surface area of 3425 m^2/g and a total pore volume of 2.44 cm^3/g. The pore size distribution obtained from the N_2 adsorption data at 77 K and mercury porosimetry show the presence of a highly developed porous structure containing micropores, mesopores and macropores. The elemental analysis of the VR residue shows preferentially hydrogen (10.4%) and sulfur (3.8%) as the main components besides carbon (85.2%).

In a first step, the PP-AC has been evaluated in the adsorption of an aromatic molecule such as methylene blue. To this end, the ASTM standard and the equilibrium adsorption isotherm have been performed. The amount of MB adsorbed after application of the ASTM method gives a final value for MB on PP-AC of 724 mg/g, and in the equilibrium process the value goes up to 950 mg/g. To our knowledge, these values are far exceeding those reported in the literature for conventional activated carbons (100-500 mg/g), thus confirming the exceptional performance of these unique petroleum-

pitch derived carbons [24-27]. Interestingly, these adsorption values for MB give rise to an estimated surface area of 2300 m^2/g (considering that each molecule of MB covers an area of 1.3 nm^2). Taking into account that MB is a large molecule with a kinetic diameter around 1.3-1.4 nm, the aforementioned observation clearly denotes an unexpected behavior in the PP-AC. For instance, taking into account that the surface area calculated for pores above 1.3 nm is around 1200 m^2/g, these results anticipate that, unexpectedly, MB is able to access pores below 1.3 nm.
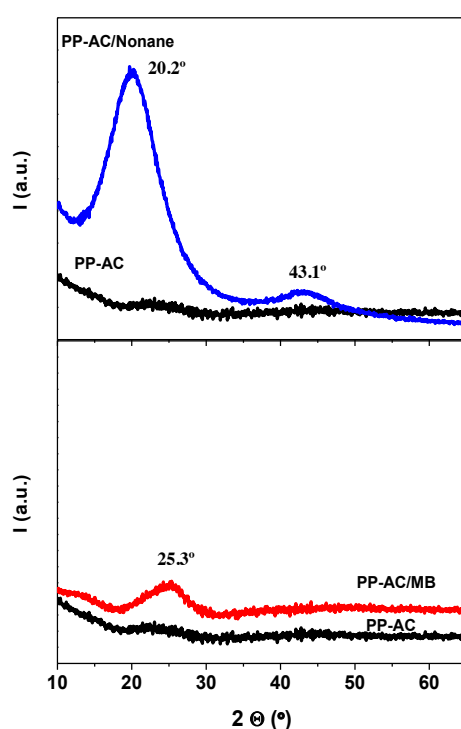
Figure 1. XRD pattern for the synthesized PP-AC sample before and after adsorption of methylene blue (MB) using and n-nonane following the procedure described in the experimental section.

To fully understand the adsorption behavior in PP-AC upon exposure to methylene blue, Figure 1 shows the XRD pattern before and after the exposure. The original PP-AC exhibits a rather flat profile with a small shoulder at 25° corresponding to the reflection of the (002) plane from graphite microdomains, in close agreement with the

graphitizable nature of the petroleum residue. However, the low crystallinity of this sample clearly denotes the destruction of the structural order after KOH activation, probably due to the intercalation of K into the lamellar structure. Contrary to our expectation, the incorporation of methylene blue into the porous structure gives rise to substantial changes. Methylene blue adsorbed in the PP-AC gives rise to an increase in the intensity in the 25.3° XRD line. These results can be explained either due to an epitaxial adsorption of MB in the graphitic crystallites of the micropore/mesopore wall or to the reorientation of the graphitic carbon domains upon adsorption. Although this observation is rare for activated carbons, similar changes in the XRD pattern were described by Suzuki *et al*. upon benzene adsorption on activated carbon fibers [28]. To discard any effect due to the epitaxial adsorption of the aromatic ring on the graphitic walls, the XRD analysis have been extended to a non-planar and larger organic molecule, as n-nonane. As it can be observed in Figure 1, adsorption of n-nonane in the carbon structure gives rise to a more drastic effect compared to MB. Adsorption of n-nonane gives rise to a very significant increase in the intensity of the (002) diffraction peak and a shift to lower 2 theta values (20.2°). Furthermore, the XRD pattern also shows a broad peak at 43.1° that can be unambiguously attributed to the overlap reflections from (100) and (101) in graphite.

These results clearly anticipate that MB and n-nonane pre-adsorption give rise to a rearrangement of the carbon structure with the interlayer spacing ranging from 0.356 nm to 0.420 nm after MB and n-nonane incorporation, respectively. At this point it is important to highlight that these results are unique for petroleum-derived activated carbons and clearly reflect the presence of reorientation processes for the graphite domains. Presumably, the carbon is able to adapt its skeleton to accommodate the guest molecule upon adsorption. At this point it is important to highlight that similar

experiments in lignocellulose-derived activated carbons (e.g., olive stones derived activated carbons) did not give rise to any appreciable change in the XRD profile upon MB or n-nonane adsorption. The macroscopic effect of this internal reorientation and the associated flexibility can be appreciated in Figure S1, with a clear contraction of the PP-AC carbon after incorporation of an aqueous solution containing MB.

Further evidence of the anomalous adsorption performance in petroleum-pitch activated carbon can be obtained after application of immersion calorimetry. In the absence of specific interactions at the solid-liquid interface, the heat of immersion ($-\Delta H_{imm}$) into a certain liquid can be correlated with solid surface area available for this molecule [18]. To exclude any possibility of specific interaction with the solid surface, two hydrocarbon molecules have been selected for the calorimetric measurements: benzene (kinetic diameter of 0.37 nm) and alpha-pinene (kinetic diameter of 0.7 nm). Table 1 shows a comparison of the enthalpy values for the PP-AC and a conventional activated carbon (AC) obtained from olive stones (using chemical activation with $ZnCl_2$ followed by physical activation with CO_2).

Table 1. Enthalpy of immersion (J/g) for sample PP-AC and a conventional activated carbon from olive stones.

Sample	*Bz*	*α-pinene*
	$-\Delta H_{imm}$ (J/g)	$-\Delta H_{imm}$ (J/g)
PP-AC	278	292
AC	177	167

In the specific case of the conventional activated carbon (sample AC) the enthalpy of immersion for both hydrocarbons remains in between 160-180 J/g, these values being

very similar to those reported by our research group for carbide-derived carbons and physically activated carbon derived from olive stones [29,30]. On the contrary, the values achieved for the PP-AC sample are somehow unexpectedly high. The values obtained for the petroleum-pitch carbons using both hydrocarbons approach 300 J/g, these values being even larger than those reported for materials like zeolites with a rich surface chemistry [18]. Consequently, calorimetric results suggest that the exposure of this type of petroleum-derived carbon materials to liquid hydrocarbons (either aromatic and non-aromatic) does not only imply simple wettability processes. Other phenomena must be taken into consideration to explain the high calorimetric values (for instance structural changes or graphite domain reorientation).

To gain further insight into the nature of the structural flexibility in carbon materials and the adsorption state of n-nonane in the inner cavities of the carbon sample, PP-AC has been evaluated using inelastic neutron scattering (INS) upon exposure to n-nonane and after a subsequent exposure to high-pressure methane. INS spectra were measured at TOSCA beamline at the Rutherford Appleton Laboratory (UK). INS is especially sensitive to the dynamics of hydrogen and hydrogen-bearing groups due to the relatively large incoherent neutron cross-section of hydrogen compared to other atomic nuclei. Consequently, it is a powerful tool for the evaluation of the vibrational and rotational modes of hydrocarbons confined in nanoporous materials, upon external stimuli. Figure S2 shows the INS spectra corresponding to the sample saturated with n-nonane, i.e. PP-AC containing n-nonane in all cavities.

As it can be observed in the experimental profile, n-nonane adsorbed in the cavities of the carbon material shows the characteristic peaks of the un-confined hydrocarbon with the high longitudinal acoustic modes (LAM), that is the lowest frequency molecular vibrations involving extension of the alkane chains, above 200 cm^{-1}, and the transverse

acoustic modes (TAM), lower frequency LAM´s and the external modes, below 200 cm^{-1} [31,32]. Figure S2 also includes the calculated spectra for n-nonane obtained using the mixed Monte Carlo multiple minimization and Large Scale Low mode method, as implemented in the MacroModel software. Structural assignments were based primarily on the level of correspondence between the experimental and computed wavenumbers, and on their calculated relative energies. As observed in Figure S2, the agreement between experiment and theory is very good, and this was obtained for the calculated minimum energy structure, i.e., even the single molecule *ab initio* calculations of the vibrational frequencies provides an excellent agreement with the INS spectrum. Theoretical calculations perfectly predict the strong peak at 240 cm^{-1}, due to the methyl torsion, and peaks at 290, 396, 455 and 497 cm^{-1}, attributed to in-plane longitudinal acoustic modes. Only out-of-plane transverse acoustic modes below 200 cm^{-1} exhibit a worse fitting with the experimental data. The optimized geometry and harmonic vibrational frequencies for the lowest energy structure are given as Electronic Supplementary Information (Table S1, S2).

Figure 2 describes the INS spectrum for the activated carbon PP-AC after an outgassing treatment at 298 K for 4h.
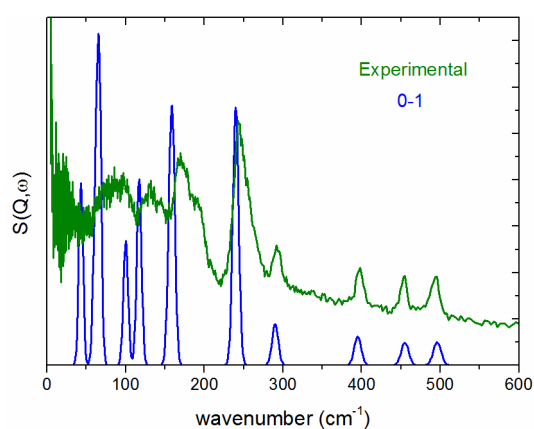
Figure 2. Experimental INS spectrum (green trace) of nanoporous activated carbon pre-impregnated with n-nonane and outgassed at RT for 4h. Theoretical INS spectrum (blue trace) of the fundamental modes (0-1) of the lowest energy conformer of n-nonane molecule.

Previous studies from our research group have shown that an outgassing treatment under these conditions allows the removal of n-nonane from the whole porosity, except from narrow micropores (below 1 nm) [33]. As it can be observed in the experimental spectra, n-nonane molecules confined in the narrow micropores of the activated carbon retain the longitudinal acoustic modes (LAM), while all contributions below 200 cm^{-1} are mainly wash-out. These results show that the methyl torsional and in-plane acoustic modes of n-nonane confined in narrow micropores remain intact, while out-of-plane contributions are somewhat broadened (due to the slight disorder of the confined n-nonane molecules). To evaluate any possible structural flexibility in sample PP-AC upon an external stimuli, INS analysis of confined n-nonane were evaluated after a pressurization step with CH_4 up to 6 MPa. Figure 3 shows the INS spectra of n-nonane confined in narrow micropores, before and after exposure to high-pressure methane. Interestingly, the application of high-pressure methane has no effect in the LAM acoustic modes (above 200 cm^{-1}). However, a closer look to the low wavenumber region (see highlighted area) clearly shows that an external pressurization in the reaction chamber allows sharpening of the out-of-plane acoustic modes, preferentially those at 194, 176, 165 and 133 cm^{-1}. These results unambiguously denote a certain ordering of the confined n-nonane molecules towards the crystalline phase.
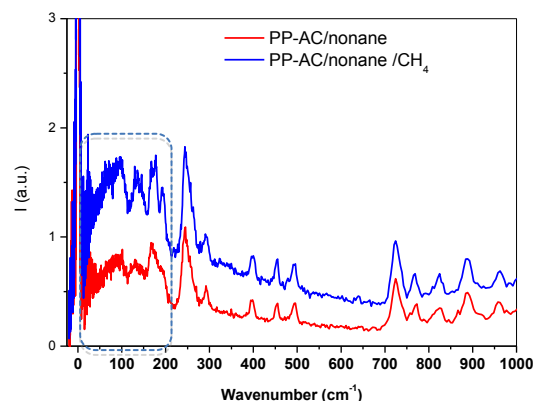
Figure 3. INS spectra of n-nonane adsorbed in narrow micropores before and after pressurization with 6 MPa CH$_4$.

In summary, INS results show that the bands corresponding to the out-of-plane acoustic modes of n-nonane become broader upon confinement in narrow micropores. However, the application of an external high-pressure stimulus allows the sharpening of these acoustic modes. The ordering of confined n-nonane upon pressure can be explained either due to the partial displacement of n-nonane from narrow micropores to wider pores or due to the partial swelling of the carbon structure. To evaluate these two hypotheses, MD simulations were performed in a model carbon material after incorporation of n-nonane in narrow micropores and high-pressure methane in the larger cavities and/or the external surface.

MD simulations predict a double layer for n-nonane adsorbed in narrow micropores (1 nm) with a packing density rather closed to the solid state. Under these conditions, vibrational and rotational modes for n-nonane will be limited in close agreement with INS measurements. Incorporation of high-pressure methane (6 MPa) into the large carbon cavities (simulated mesopores $\approx$ 8 nm) gives rise to some methane dissolution in n-nonane, but associated with a full preservation of the solid n-nonane stability in

narrow micropores (see snapshot in Figure 4; see Supporting information for further details), i.e. MD simulation does not predict any change in the n-nonane adsorbed in narrow micropores neither in the carbon porous structure (a rigid pore model was chosen to avoid ambiguity in terms of potential and the simulation). Consequently, these calculations suggest that the sharpening of the acoustic modes after application of a high-pressure stimulus must be undoubtedly attributed to the structural flexibility (swelling) of the PP-AC activated carbon, which allows somewhat disordered structure of n-nonane within micropores to rearrange further towards the crystalline phase.
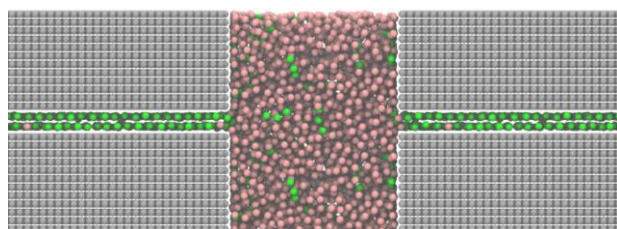
Figure 4. Snapshot of the MD simulations for a model carbon material containing n-nonane (green) in small cavities (1 nm) and high-pressure methane (brown) in large cavities (8 nm).

To conclude the characterization, sample PP-AC has been evaluated using TEM after MB adsorption. One of the main drawbacks for the observation of these samples after pre-impregnation with MB concerns the high vacuum in the TEM chamber and high energy of the electron beam, preferentially at high magnification. Figure 5 shows TEM images from different areas of the carbon surface immediately after focusing (upper pictures) and after a few seconds bombardment with the electron beam (lower pictures). TEM images clearly show the detrimental effect of the electron beam in the pre-impregnated sample. Whereas the initial pictures allows observing the carbon skeleton (MB adsorbed can not be appreciated), the surface structure changes drastically after a

few seconds exposure. All pictures show the presence of defective areas due to the presence of "explosion-like" processes. We assume that these crater formation must be associated with the abrupt desorption of MB from the inner cavities of the PP-AC carbon assisted by the electron beam.
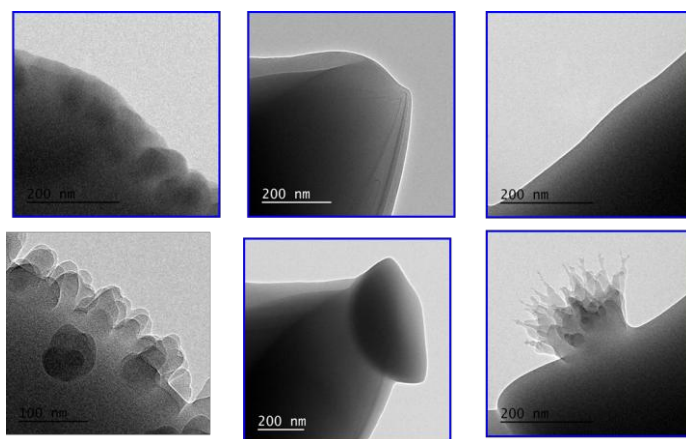

Figure 5. TEM images of the PP-AC sample pre-impregnated with an aqueous solution of methylene blue right after focusing (upper section) and after a few seconds under the electron beam (lower section).

Interestingly, after the explosion phenomenon TEM images show the formation of a new solid structure emerging from the carbon core, most probably attributed to the exfoliation of graphite micro-domains or graphene layers (Figure 5). This hypothesis will be in close agreement with structural flexibility described above for these petroleum-pitch activated carbons and it anticipates the possibility to use these carbon materials for the preparation of graphene flakes. However, the presence of some amorphous domains coming from the decomposition of the MB molecules after irradiation cannot be ruled out.

To demonstrate the structural flexibility and the weakness of the interaction of the lamellae in PP-AC observed with TEM, the carbon sample has been submitted to an exfoliation process using two different organic solvents, N,N-dimethylformamide (DMF) and N-methyl-2-pyrrolidone (NMP). For the exfoliation process, the impregnated sample was sonicated for 15 min and subsequently diluted in ethanol before their evaluation using atomic force microscopy (AFM). Figure 6 shows the AFM images corresponding to the PP-AC sample exfoliated using NMP. As it can be observed, exfoliation gives rise to μm size graphene flakes (see Figure 6 upper panel). A closer look to these graphene flakes (amplification in the middle image) shows the presence of surface imperfections or pore cavities around 50-100 nm in size. A topological analysis of these flakes along the vertical axes (blue line) reflects that they are indeed constituted by 1-3 stacked graphene layers with a height around 1.5 nm. At this point it is important to highlight that similar exfoliation experiments using DMF did not succeed to produce graphene.

The morphology of the synthesized graphene samples can be more clearly appreciated in Figure S5. AFM pictures clearly show that upon exfoliation i) the graphene particles exhibit an average size around 500 nm-1000 nm in diameter, ii) graphene planes contain pores with an average size around 50-100 nm, iii) graphene flakes exhibit rough and rounded boundaries and iv) topological analysis of these flakes along the vertical axes following the blue lines (a-c) show that each of the two-three layers is less than 1 nm height (ca. 0.6±0.1 nm), i.e. these are single graphene monolayers.
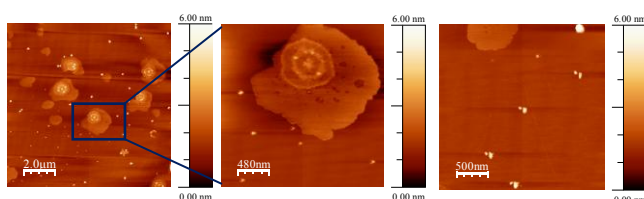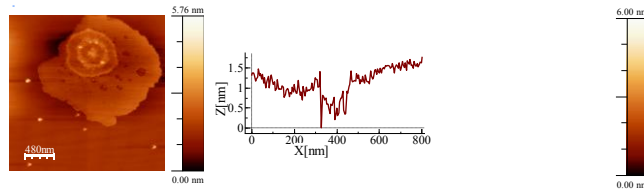
Figure 6. AFM pictures and height profiles corresponding to the exfoliated PP-AC activated carbon.

These results suggest that the KOH activation process in these anisotropic samples must proceed via potassium intercalation between the graphitic domains followed by an activation reaction, i.e. the reaction of KOH with the pitch starting from the periphery of the flakes to the core giving rise to the evolution of CO, CO_2 and H_2 (see ref. [34] for further details), thus providing the rough and heterogeneous "egg-like" flake graphene structure, as observed with AFM. The "egg-like" flake morphology of these samples is supported by SEM images after exfoliation and drying. Figure 7 clearly shows the compilation of micron-size graphene layers.
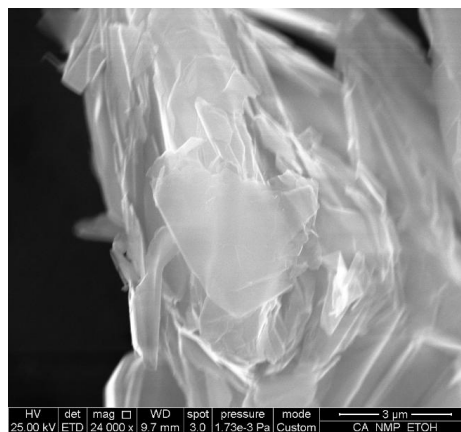

Figure 7. SEM image of the petroleum-pitch activated carbon after exfoliation and drying.

To end up, it is important to highlight that this exfoliation approach was applied to other petroleum-pitch derived carbon materials with similar results in terms of final graphene-flakes structure and morphology.

4. Conclusions

This study clearly shows that petroleum-pitch derived carbons are excellent candidates for the preparation of graphene through a simple exfoliation process, avoiding the drawbacks associated with the conventional routes from graphite based on an initial oxidation, followed by a dangerous thermal reduction step. The large versatility of these activated carbon samples must be associated to the increased structural flexibility upon adsorption, i.e. the ability of the material to adapt to the guest molecule, via an internal rearrangement/reordering of the graphite microdomains, as described by XRD. These internal structural changes can be responsible for the excellent performance of these materials in applications dealing with adsorption and capacitance.

Notes and references

[1] Rouquerol J, Rouquerol F, Llewellyn P, Maurin G, Sing KSW, *Adsorption by powders and porous solids*, 2nd Ed., Elsevier, 2012.

[2] Thommes M, Kaneko K, Neimark AV, Olivier JP, Rodríguez-Reinoso F, Rouquerol F, Sing KSW. Physisorption of gases, with special reference to the evaluation of surface area and pore size distribution (IUPAC Technical Report). Pure Appl Chem 2015; 87: 1051-69.

[3] Casco ME, Cheng YQ, Daemen LL, Fairén-Jimenez D, Ramos-Fernández EV, Ramirez-Cuesta AJ, et al. Gate-opening effect in ZIF-8: the first experimental proof using inelastic neutron scattering. Chem Commun 2016; 52: 3639-42.

[4] Neimark AV, Coudert FX, Boutin A, Fuchs AH. Stress-based model for the breathing of metal-organic frameworks. Chem Letter 2010; 1: 445-9.

[5] Kowalczyk P, Furmaniak S, Gauden PA, Terzyk AP. Methane-induced deformation of porous carbons: From normal to high-pressure operating conditions. J Phys Chem C 2012; 116: 1740-47.

[6] Long Y, Palmer JC, Coasne B, Sliwinska-Bartkowiak M, Jackson G, Müller EA, et al. On the molecular origin of high-pressure effects in nanoconfinement: The role of surface chemistry and roughness. J Chem Phys 2013; 139: 144701.

[7] Balzer C, Wildhage T, Braxmeier S, Reichenauer G, Olivier JP. Deformation of porous carbons upon adsorption. Langmuir 2011; 27: 2553-60.

[8] Kowalczyk P, Ciah A, Neimark A. Adsorption-induced deformation of microporous carbons: Pore size distribution effect. Langmuir 2008; 24: 6603-08.

[9] Balzer C, Braxmeier S, Neimark AV, Reichenauer G. Deformation of microporous carbon during adsorption of nitrogen, argon, carbon dioxide, and water studied by in situ dilatometry. Langmuir 2015; 31: 12512-19.

[10] Do DD, Nicholson D, Do HD. Effects of adsorbent deformation on the adsorption of gases in slitlike graphitic pores: A computer simulation study. J Phys Chem C 2008; 112: 14075-89.

[11] Gor GY, Paris O, Prass J, Russo PA, Ribeiro Carrott MML, Neimark A. Adsorption of n-pentane on mesoporous silica and adsorbent deformation. Langmuir 2013; 29: 8601-08.

[12] Ravikovich PI, Neimark A. Density functional theory model of adsorption deformation. Langmuir 2006; 22: 10864-68.

[13] Reichenauer G, Scherer GW. Extracting the pore size distribution of compliant materials from nitrogen adsorption. Colloids Surf A: Phys Eng Aspects 2011; 187: 41-50.

[14] Casco ME, Martínez-Escandell M, Gadea-Ramos E, Kaneko K, Silvestre-Albero J, Rodríguez-Reinoso F. High-pressure methane storage in porous materials: Are carbon materials in the pole position?. Chem Mater 2015; 27: 959-64.

[15] Casco ME, Martínez-Escandell M, Silvestre-Albero J, Rodríguez-Reinoso F. Effect of the porous structure in carbon materials for CO_2 capture at atmospheric and high-pressure. Carbon 2014; 67: 230-5.

[16] Mora E, Ruiz V, Santamaria R, Blanco C, Granda M, Menéndez R, et al. Influence of mesophase activation conditions on the specific capacitance of the resulting carbons. J Power Sources 2006; 156: 719-24.

[17] Silvestre-Albero A, Gonçalves M, Itoh T, Kaneko K, Endo M, Thommes M, et al. Well-defined mesoporosity on lignocellulosic-derived activated carbons. Carbon 2012; 50: 66-72.

[18] Silvestre-Albero J, Gómez de Salazar C, Sepúlveda-Escribano A, Rodríguez-Reinoso F. Characterization of microporous solids by immersion calorimetry. Colloids Surf A: Phys Eng Aspects 2001; 187-188: 151-65.

[19] Parker SF, Fernandez-Alonso F, Ramirez-Cuesta AF, Tomkinson J, Rudic S, Pinna RS, et al. Recent and future developments on TOSCA at ISIS. J Physics: Conference Series 2014; 554: 012003.

[20] Frisch MJ, Trucks GW, Schegel HB, et al. Gaussian 09, Revision B.01, Gaussian, Inc., Wallinford, CT, 2010.

[21] Ramirez-Cuesta AJ. aCLIMAX 4.0.1, The new version of the software for analysing and interpreting INS spectra. Computer Physics Communications 2004; 157: 226-38.

[22] Herdes C, Totton TS, Müller EA. Coarse grained force field for the molecular simulation of natural gases and condensates. Fluid Phase Equilibria 2015; 406: 91-100.

[23] Müller EA, Jackson G. Force-field parameters from the SAFT-γ equation of state for use in coarse-grained molecular simulations. Annual Rev Chem & Biomol Eng 2014; 5: 405-27.

[24] He X, Male KB, Nesterenko PN, Brabazon D, Paull B, Luong JHT. Adsorption and desorption of methylene blue on porous carbon monoliths and nanocrystalline cellulose. ACS Appl Mater Interf 2013; 5: 8796-804.

[25] Rodriguez A, García J, Ovejero G, Mestanza M. Adsorption of anionic and cationic dyes on activated carbon from aqueous solutions: equilibrium and kinetics. J Haz Mater 2009; 172: 1311-20.

[26] Pezoti O, Cazetta AL, Souza IPAF, Bedin KC, Martins AC, Silva TL, et al. Adsorption studies of methylene blue on $ZnCl_2$-activated carbon produced from buriti shells. J Indus & Eng Chem 2014; 20:4401-4407.

[27] Foo KY, Hameed BH. Utilization of rice husks as a feedstock for preparation of activated carbon by microwave induced KOH and K2CO3 activation. Bioresource Techn 2011; 102:9814-9817.

[28] Suzuki T, Kaneko K. Structural change of activated carbon fibers with desorption by in situ X-ray diffraction. Carbon 1988; 26: 743-5.

[29] Silvestre-Albero A, Rico-Francés S, Rodríguez-Reinoso F, Kern AM, Klumpp M, Etzold BJM, et al. High selectivity of TiC-CDC for CO_2/N_2 separation. Carbon 2013; 59: 221-8.

[30] Silvestre-Albero J, Silvestre-Albero A, Rodríguez-Reinoso F, Thommes M. Physical characterization of activated carbons with narrow microporosity by nitrogen (77.4 K), carbon dioxide (273 K) and argon (87.3 K) adsorption in combination with immersion calorimetry. Carbon 2012; 50: 3128-33.

[31] Braden DA, Parker SF, Tomkinson J, Hudson BS. Inelastic neutron scattering spectra of the longitudinal acoustic modes of the normal alkanes from pentane to pentacosane. J Chem Phys 1999; 111: 429.

[32] Tomkinson J, Parker SF, Braden DA, Hudson BS. Inelastic neutron scattering spectra of the transverse acoustic modes of the normal alkanes. Phys Chem Chem Phys 2002; 4: 716-21.

[33] Oschatz M, Borchardt L, Rico-Francés S, Rodríguez-Reinoso F, Kaskel S, Silvestre-Albero J. Textural characterization of micro- and mesoporous carbons using combined gas adsorption and n-nonane preadsorption. Langmuir 2013; 29: 8133-39.

[34] Martinez-Escandell M, Monteiro de Castro M, Molina-Sabio M, Rodríguez-Reinoso F. KOH activation of carbon materials obtained from the pyrolysis of ethylene tar at different temperatures. Fuel Proc Techn 2013; 106: 402-7.